ES Food and Agroforestry
DOI: https://dx.doi.org/10.30919/faf1415

Jamun Seed (*Syzygium Cumini*) Biochar as a Potential Adsorbent for Environmental Applications

Asha Ripanda,[1,*] Mwemezi J Rwiza,[2] S. Giridhar Reddy,[3,*] Elias Charles Nyanza,[4] Ramadhani Bakari,[5] Hossein Miraji,[1] C. R. Ravikumar,[6] H. C. Ananda Murthy,[7, 8] Saidi Ali Hamad Vuai,[9] Revocatus L. Machunda[2] and Sri Hari Kumar Annamareddy[10]

Abstract

This study investigates the properties and adsorption performance of jamun seed biochar (JS biochar) produced through calcination at varying temperatures. Elemental analysis reveals that the carbon content significantly increases from 64.25 to 87.93 wt.% as calcination temperature rises from 400 to 600 °C, while nitrogen content remains within the range of 2 to 2.29 wt.%. The biochar's surface characteristics, with a maximum specific surface area of 261.2 m^2/g, demonstrate strong adsorption capacity for small organic molecules, including ciprofloxacin (555.55 mg/g) and lamivudine (400 mg/g). The identified functional groups, including hydroxyl and carbonyl groups, enhance adsorption through mechanisms such as hydrogen bonding and electrostatic interactions. The observed porous, rough surface morphology supports the material's effectiveness as an adsorbent. The results demonstrate JS biochar's high adsorption capacity, governed by a synergistic interplay of physisorption and chemisorption. This research underscores the potential of JS biochar as a sustainable and effective solution for environmental remediation, particularly in mitigating aqueous pollutants. The findings offer valuable insights for optimizing biochar properties to improve adsorption efficiency, thereby promoting sustainable waste management and environmental remediation.

Keywords: Syzygium cumini; Environmental remediation; Water pollution; Biomass-based adsorbents; Surface properties.
Received: 24 December 2024; Revised: 08 January 2025; Accepted: 20 January 2025.
Article type: Research article.

1. Introduction

The contamination of ecosystems with organics, such as antibiotics, and inorganics, such as lead, continues to threaten the environment and public health.[1-3] These substances are recognized as pollutants due to their widespread use and improper disposal.[4-8] The pollution due to these substances primarily originates from industries, pharmaceutical waste, agricultural runoff, healthcare facilities, and household products,[4-9] leading to the persistent presence in soil and water bodies,[5, 10-13] and linked with deterioration of ecological health.[4-8,14] Additionally, water pollutants such as ciprofloxacin, lamivudine, lead, and chromium can disrupt natural microbial communities, leading to ecological imbalances.[15,16] Non-target organisms, including beneficial microbes essential for nutrient cycling and ecosystem functioning, are particularly vulnerable. Addressing water pollution requires innovative and sustainable approaches.[9,17]

Among various remediation strategies, the use of biomass-based adsorbents has gained attention for its effectiveness, environmental friendliness, and cost-efficiency. Biomass-based adsorbents are derived from renewable organic materials such as agricultural residues, forestry by-products, and other organic wastes. These materials are not only abundant and inexpensive but also possess unique properties that make them highly effective for polluted water remediation. Furthermore, exposure to sub-lethal concentrations of organic pollutants such as ciprofloxacin to microbes may result in the

[1] Department of Chemistry, College of Natural and Mathematical Sciences, University of Dodoma, P.O. Box 338, Dodoma, 11090, Tanzania
[2] School of Materials, Energy, Water and Environmental Sciences (MEWES), P.O. Box 447, The Nelson Mandela African Institution of Science and Technology (NM-AIST), Tengeru Campus, Arusha, 23100, Tanzania
[3] Department of Physical Sciences, Amrita School of Engineering, Bengaluru Campus, Amrita Vishwa Vidyapeetham, Bengaluru, 560035, India
[4] Department of Environmental and Occupational Health, School of Public Health, Catholic University of Health and Allied Sciences (CUHAS), Mwanza, 1464, Tanzania

development of resistance mechanisms, rendering standard treatments ineffective. This resistance can spread among microbial communities, posing a severe threat to human and other animal health by making infections harder to treat. The Centers for Disease Control and Prevention (CDC) estimates that more than 2.8 million antimicrobial-resistant infections occur in the U.S. annually, with around 700,000 deaths worldwide due to antimicrobial resistance (AMR).[18-20] Similarly, inorganic pollutants such as heavy metals can play a significant role in the development and spread of AMR. This interaction occurs because certain heavy metals, when present in high concentrations, can co-select for antibiotic resistance in microorganisms and thus disrupt ecological health.[21,22] Among the most toxic heavy metals, cadmium, mercury, lead, and arsenic have contributed to AMR.[21] Long-term exposure to these metals, especially in aquatic and soil environments, can lead to widespread resistance in bacteria, leading to the deterioration of ecological health. Thus, measures are required for ecological safety and sustainability.

Fig. 1: Jamun plant (Syzygium cumini) with its fruits.

[5] *Department of Petroleum and Energy Engineering, The University of Dodoma, P.O. Box, Dodoma, 11090, Tanzania*

[6] *Research Centre, Department of Chemistry, East West Institute of Technology, Bangalore, 560091, India*

[7] *Department of Applied Sciences, Papua New Guinea University of Technology, Lae, Morobe, Province, 411, Papua New Guinea*

[8] *Department of Prosthodontics, Saveetha Dental College and Hospital, Saveetha Institute of Medical and Technical Science (SIMAT), Saveetha University, Chennai, Tamil Nadu, 600077, India*

[9] *Mbeya University of Science and Technology, Mbeya, 5311, Tanzania*

[10] *Department of Chemical and Petrochemical Engineering, University of Nizwa, Birkat Al-Mouz, 616, Sultanate of Oman*

**Email:* asha.ripanda@udom.ac.tz (A. Ripanda); s_giri@blr.amrita.edu (G. Reddy)

Adsorption using biomass-based materials such as *Syzygium cumini* seeds (Fig. 1) involves the physical or chemical binding of contaminants onto the adsorbent. These materials are naturally porous and contain functional groups (such as hydroxyl, carboxyl, and phenolic groups) that enhance their interactions with various water pollutants, including organics such as ciprofloxacin and inorganics such as lead and mercury. High adsorption capacity, renewability, and biodegradability make biomass-based adsorbents particularly suitable for removing persistent low levels of pollutants and reducing the environmental impacts associated with their production and disposal. Additionally, utilizing waste materials for adsorbent production contributes to waste management and promotes circular economy principles. For example, agricultural wastes like rice husks, coconut shells, and corn cobs, which are often discarded, can be converted into valuable adsorbents. The process of creating biomass-based adsorbents typically involves simple and low-cost methods such as drying, grinding, thermal or chemical activation or even pyrolysis to produce the carbon nanostructures.

Furthermore, biomass-based adsorbents can be modified to enhance their adsorption properties. Chemical treatments or the addition of functional groups can tailor the adsorbents for specific contaminants, improving their efficiency and effectiveness. Table 1 presents studies that used biochar made from jamun (*Syzygium cumini*) seed biomass, type of pollutant, conditions, removal or adsorption capacity. Co-selection between heavy metals and antimicrobial resistance presents a significant challenge, as antimicrobial pollution promotes resistance and disrupts ecological balance. Therefore, effective remediation strategies are essential to mitigate these impacts. Biomass-based adsorbents offer a promising solution due to their sustainability, cost-effectiveness, and high adsorption capacity, making them an attractive alternative to traditional methods. By utilizing natural materials and simple production techniques, biomass-based adsorbents provide an eco-friendly and efficient approach to addressing the pervasive issue of pollution. As research and development in this field progress, the adoption of biomass-based adsorbents could play a crucial role in safeguarding both environmental and public health.[6,23-30]

The Jamun plant (*Syzygium cumini*), also known as the Java plum or Indian blackberry, is indigenous to the Indian subcontinent.[31] It is native to regions of India, Bangladesh, Nepal, Sri Lanka, and parts of southeast Asia, including Thailand and Philippines. The tree is also found in other tropical and subtropical regions due to its adaptability,[31] and its fruits are underutilized. Jamun seed biomass for the preparation of adsorbent has several advantages compared to its leaves or bark.[32] Fruit yield for full-grown seedlings ranges from 80-100 kg and 60-70 kg for grafted plants per year, indicating the potential source of seed biomass for adsorbent preparation.[33] Seeds have a higher carbon content compared to leaves and bark, which is beneficial for producing high-

Table 1: Studies that used biochar prepared from jamun (*Syzygium cumini*) seed biomass for remediation, type of pollutant, conditions, removal, or adsorption capacity reached.

Biomass	Pollutant	Conditions	Removal/Adsoption capacity	Remarks	Reference
Jamun (*Syzygium cumini*) seed	Pb (II) ions	NaOH	99.91% of Pb(II) was removed from aqueous solution	Potential use for remediation of lead contaminated water and effluents	[23]
	Fluoride	KOH, H_3PO_4, $ZnCl_2$ pyrolysis at 900 °C	Maximum adsorption capacity of 3.65 mg g^{-1}	Potential use for remediation of other pollutants	[24]
	Cr (VI)	NaOH	The Bed Depth Service Time (BDST) model was appropriate for designing the column for industrial purposes		[25]
	As (III)	$FeCl_3$, NaOH, HCHO, H_2SO_4, HCl	Maximum percent removal of 69.30 % to 88 % of As (III) was achieved	Potential use for remediation of arsenic contaminated water and effluents	[26]
	Fe (II)	Physical, chemical and combined physio-chemical treatment	The maximum adsorption capacity of 266.9 mg/g, following Pseudo first order kinetics	Potential use for remediation of iron contaminated water and effluents	[27]
	Fuchsin dye	Pyrolysis at 500 °C	The maximum adsorption capacity for BF dye was found with jamun seed biochar produced at 500 °C	Potential for remediation of other organic pollutants	[28]
	Ciprofloxacin, lamivudine	pyrolysis at 400, 500, 600 and 750 °C	More than 90% removal with the model predicting up to 100% removal	Potential for remediation of water and wastewater contaminated with organic pollutants	[6, 29, 30]

quality activated carbon.[34] The cellular structure of the seeds often leads to the formation of a more porous adsorbent material, which can enhance the adsorption capacity.

Jamun seeds contain phenolic compounds and fibers that might contribute to better adsorptive properties for the effective removal of contaminants.[35] Jamun seeds are often considered a waste product after the fruit is consumed, utilizing them for adsorbent preparation adds value to this byproduct and reduces waste.[36] Seeds provide a more uniform and stable raw material compared to leaves and bark, which can vary significantly in composition and structure based on environmental conditions.[34] Therefore, adsorbents made from seeds are often more durable and have a longer operational life compared to leaves or bark,[36] which can degrade more quickly. Since seeds are a byproduct and often available in large quantities, the cost of obtaining raw material for adsorbent preparation is low.[37] Table 2 summarizes data on how different biomass-based adsorbents perform under specific conditions, providing insights into their efficiency in the remediation of various water pollutants, including organics and inorganics. These data indicate that Jamun seed biomass is a preferable choice for preparing adsorbents for remediation. Biomass-based adsorbents can be regenerated and reused multiple times. This recyclability reduces the overall cost and environmental footprint associated with water pollution remediation processes. Biomass-based adsorbents offer a promising solution for the remediation of water pollutants due to their sustainability, cost-effectiveness, high adsorption capacity, and environmentally friendly nature. Studies are required on the application of biomass-based adsorbent for remediation of organics and inorganics in environmental settings such as urban receiving water and wastewater as most of the studies considered synthetic environments.[38-45]

2. Experimental process

Jamun seed biochar adsorbents were prepared. The sample

Table 2: Removal of antimicrobials and other organics by adsorption, biomass used to prepare adsorbent, adsorbate targeted, structure of pollutants, removal efficiency, activation agent, implication, and conditions.

Adsorbent	Adsorbate	Structure	% Removal efficacy	Activation	Implication	Conditions	Reference
Peanut husk	Amoxicillin, & tetracycline	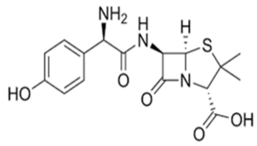	More than 70	$ZnCl_2$	Potential adsorbent for remediation of organics	pH 6.5	[38]
Rice husk	Phenol	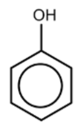	36%–64% and 28%	Ca $(OH)_2$	Potential adsorbent for remediation of organics	pH 5.58	[39]
Rice husk	Phenol		36%–64% and 28%	Thermal	Potential adsorbent for remediation of organics	pH 5.58	[39]
Lotus stalk based	Norfloxacin	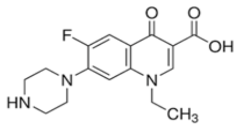	83	NaOH	Potential adsorbent for remediation of organics	pH 5.5	[40]
Macadamia nutshell	Tetracycline	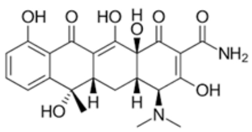	70 to 100	NaOH	Potential adsorbent for remediation of organics	pH 4 to 3	[41]
Lignin	Tetracycline		76	H_3PO_4	Future use for remediation of tetracycline	$[C]_O = 420$ mg/L; pH 5.5	[41]
Seaweed kelp	Ciprofloxacin	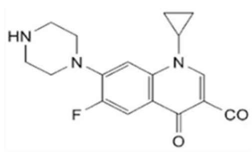	96.06%	Peroxymonosulfate	Future use for remediation of ciprofloxacin	$C_0 = 26.15 \pm 0.7$ mg kg^{-1}, pH 6.3, co-existing anions: such as Cl^-, HCO_3^-, and HPO_4^{2-}	[42]
Agricultural biomasses			Max. adsorption capacity 120.6 mg/g	H_3PO_4		Acidic pH	[43]
pumpkin peels			Max. adsorption capacity of 153.9 mg/g	H_3PO_4		HCl, pH 8, NaOH	[44]
Palm tree biomass	Rhodamine B, a tracer dye	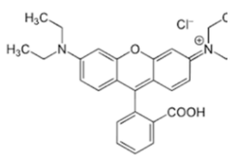	Maximum adsorption capacities of 31.81–224.30 mg/g	Not stated	Use for remediation of Rhodamine B	pH 3.4 and 7.2, 303 to 313 K, NaoH, HCL	[45]

Adsorbent	Adsorbate	Structure	% Removal efficacy	Activation	Implication	Conditions	Reference
	Metronidazole	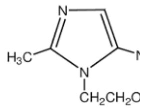	Maximum adsorption capacities of 95.44–26.76 mg/g	Not stated	Use for remediation of metronidazole		[45]

adsorbents were marked as sample 1 (calcined at 400 °C), sample 2 (calcined at 500 °C), sample 3 (calcined at 600 °C), sample 4 (calcined at 750 °C), and sample 5 (uncalcined, control), as reported by previous researchers.[29,30,46-49] This study presents the results of jamun seed biochar (JS biochar) adsorbent characterization, which was conducted after material preparation and used in a batch adsorption test to assess the efficiency for remediation of organic water pollutants (ciprofloxacin and lamivudine), as outlined in prior research.[50-54] and depicted in Fig. 2.

The batch adsorption was optimized by response surface methodology (RSM) utilizing an optimality design. Surface characteristics, such as area, volume, and pore size, were measured using a QUANTACROME 1000 L-Se series porosimeter.[42] The specific surface area and pore size distribution of the JS biochar were determined through the Brunauer Emmett Teller (BET) analysis, which relies on the physical adsorption of nitrogen gas onto the adsorbent surface.[42] A detailed methodology is provided in Ref. [20], and the data generated have been made available through Mendeley Data.[43] Additionally, the elemental composition of carbon, hydrogen, nitrogen, sulfur, and oxygen in the material was analyzed using a carbon, hydrogen, nitrogen, and sulphur (CHNS) analyzer (Flash 2000), consistent with the approach described by Manmeen and colleagues.[44]

This study builds upon and extends previous research,[6,29,30,48] where the surface functional groups of the material, both prior to and after adsorption, as well as any alterations resulting from interactions, were examined using a Perkin Elmer Fourier transform infrared (FTIR) spectroscopy (model V755).[55] High-resolution imaging and atomic-level chemical information of the JS samples were gathered using the Talos F200X G2 (S) transmission electron microscopy (TEM), a state-of-the-art instrument for detailed structural analysis.[56] Physical properties like phase composition, crystal structure, and crystal orientation in the powder form were analyzed through the Shimadzu X-ray diffraction (XRD, model 7000), a versatile, non-destructive analytical tool.[57] High magnification and resolution examination of the material's surface was conducted using a Carl Zeiss S 3400 scanning electron microscope (SEM), a German-manufactured model known for its superior imaging quality and multifunctional capabilities. Additionally, the integration of an energy-dispersive X-ray (EDX) spectroscopy with the detector allowed for the analysis of the material's elemental composition.[58]

3. Results and discussion

The data from the characterization and sorption experiments, previously shared on the Mendeley data repository and linked to the initial data article, provide valuable insights into the properties of adsorbents used for water remediation.[29,59] These results highlight the adsorbents' potential for removing both organic pollutants, like antimicrobials, and inorganic pollutants, such as lead and arsenic. Additionally, the data offer critical information on the final characterization of these adsorbents, supporting their effectiveness in environmental clean-up applications.[47]

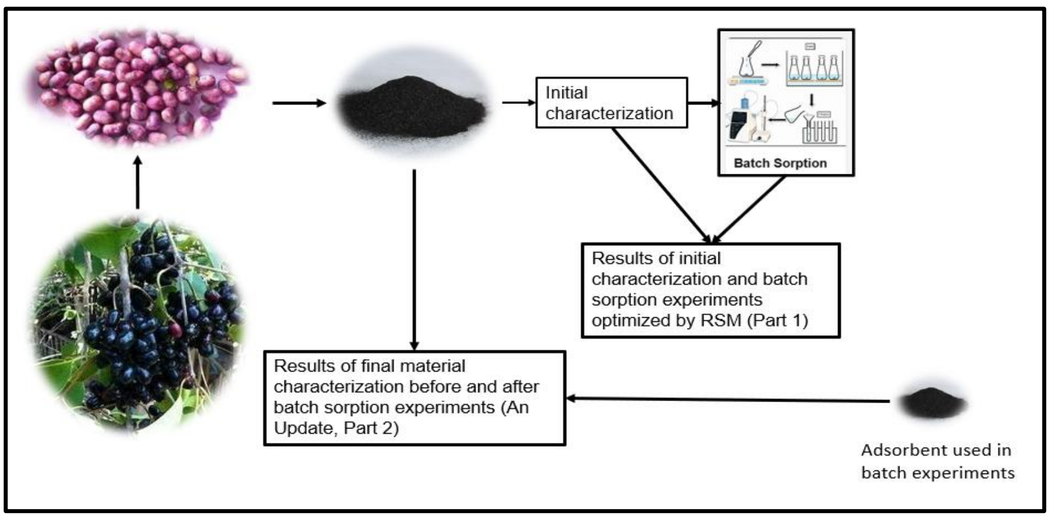

Fig. 2: Summary of methodologies presents jamun seed (*Syzygium cumini*) plant bearing seeds, dried seeds, and biochar made from seed biomass.

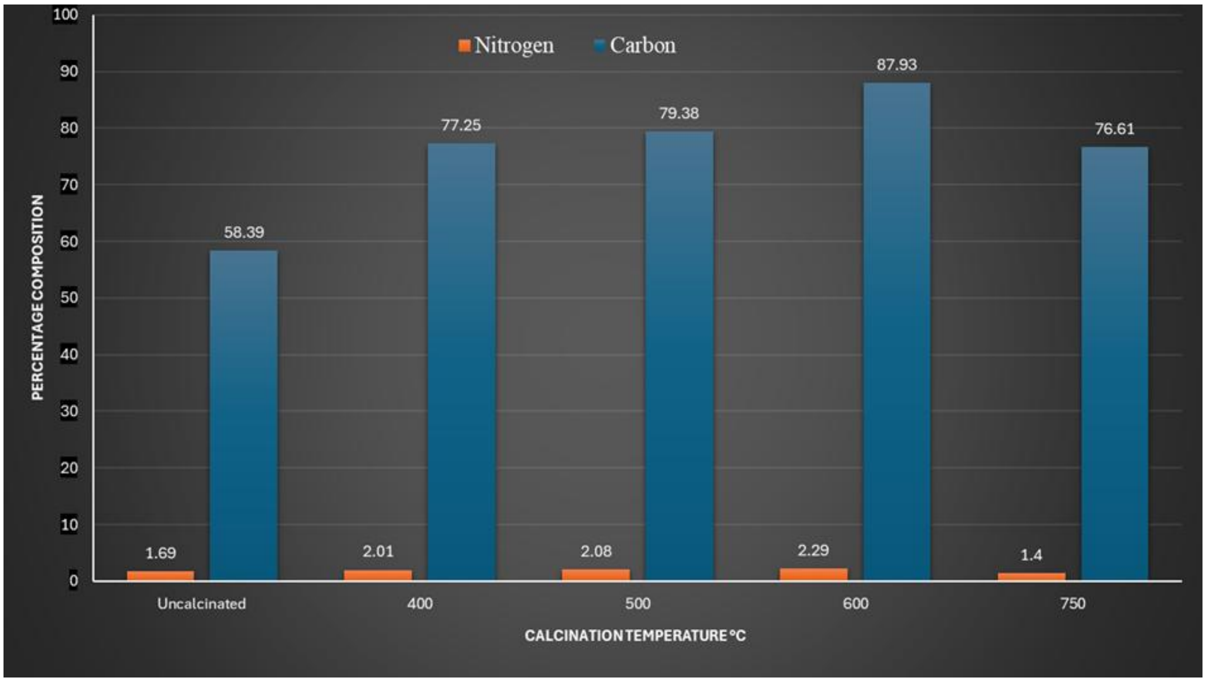

Fig. 3: Variation of carbon and nitrogen content in JS biochar samples.

3.1 Variation in carbon, nitrogen and hydrogen content

The result of elemental analysis indicates that the carbon content of JS biochar ranged from 64.25-87.93 (wt.%) and nitrogen from 2-2.29 (wt.%) when calcination temperature increased from 400 to 600 °C. The variation of carbon, nitrogen, and hydrogen in JS biochar samples are presented in Fig. 3. Increasing the temperature to 700 °C resulted in a decreased content of carbon. This trend may be due to the removal of ligands as the material is calcined. At higher temperatures, almost all ligands are removed, therefore no further increase in carbon content. Lopez and co-workers evaluated the effect of calcination temperature on the material and reported an increase in carbon content as the material was calcined from 400 to 700 °C,[60] as observed in this study.

The calcination process involves heating a material to high temperatures, leading to physical and chemical changes. Therefore, calcination can result in the removal of volatile components, decomposition of organic matter, and structural transformations. The impact on carbon content depends on the material, but in some cases, an increase in carbon content occurs as non-carbonaceous components are removed. The choice of calcination temperature influences material properties such as crystalline structure, morphology, and surface characteristics. Researchers often explore different calcination temperatures to optimize materials for specific applications such as catalysis, adsorption, and energy storage. Understanding the effects of calcination is crucial for tailoring material properties to meet desired specifications.[61] The carbon content of biochar is a critical parameter due to its significant impact on the stability, reactivity, and potential applications of biochar. High carbon content contributes to the stability of biochar, making it resistant to decomposition and increasing its potential as an adsorbent.

Similarly, the nitrogen content of biochar enhances its adsorption capacity by improving surface functionality and increasing interactions with pollutants. This makes biochar more effective in removing contaminants, such as heavy metals and organic pollutants, from water, making it a highly efficient adsorbent for environmental remediation. The nitrogen content in most adsorbents, especially biochar-based materials, typically ranges from 0.1% to 5%, JS biochar had nitrogen content within this reported range.[62] This range depends on the feedstock, production method (*e.g.*, pyrolysis), and any chemical modifications applied.[62,63] Nitrogen-enriched adsorbents often exhibit an enhanced adsorption capacity due to the presence of nitrogen-containing functional groups that interact more effectively with pollutants.

3.2 Variation of surface area, pore size and volume

Surface area, pore size, and pore volume are key characteristics of adsorbent that significantly impact material behavior. Surface area influences interactions in processes like adsorption and catalysis.[64] Pore size determines what substances can be accommodated within the material, which is crucial for applications such as gas storage and adsorptive remediation through the pore-filling mechanism.[65] Pore volume indicates the total available space within the material and directly affects its capacity for adsorption or storage.[65] These parameters play a vital role in designing and optimizing materials for specific applications, ensuring their effectiveness in processes involving gases, liquids, and other substances. The BET surface area, pore size, and volume presented in Fig. 4 indicate that the JS biochar calcined at 400 and 500 °C had similar surface properties, including the specific surface area, pore volume, and pore size. The unit of pore size is given in Angstrom, which is equal to 1×10^{-8} cm. The material calcined

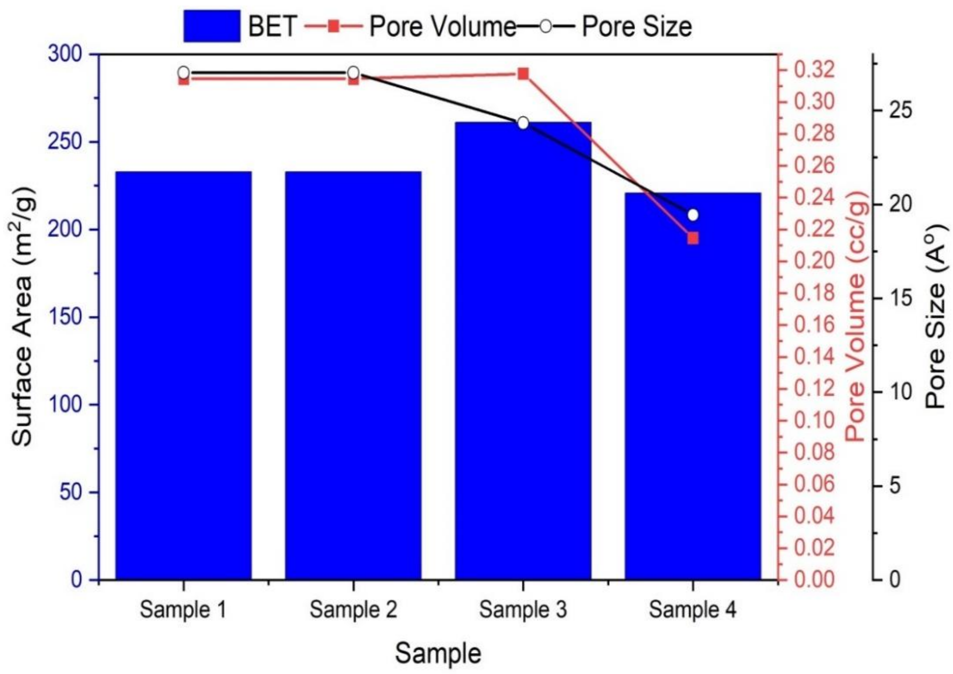

Fig. 4: Characterization data for specific surface area, pore volume, and pore size of adsorbent calcined at various temperatures.

at 600 °C had a high specific surface area and pore volume, but the pore size decreased as the calcination temperature increased to 750 °C. The present study gave the highest specific surface area of 261.2 m^2/g and adsorption capacity of 555.55 mg/g for ciprofloxacin and 400 mg/g for lamivudine adsorption with a relatively similar removal efficiency. The size and pore structure of jamun seeds biochar appear to be well-suited for adsorbing small antimicrobial molecules like lamivudine and ciprofloxacin and may potentially be used to remedy other organic and inorganic pollutants. The high removal efficiencies reported in this study suggest that the developed biochar has an appropriate pore size distribution, with sufficient micropores and mesopores to accommodate these adsorbates effectively. This makes jamun seed biochar a promising sustainable alternative to conventional adsorbents for their environmental remediation.

A similar study by Palapa *et al*.[66] reported that the composite derived from rice husk had a surface area of 200.9 m^2/g and an adsorption capacity of 470.96 mg/g. This indicates the potential of biomass-based adsorbents for the sustainable remediation of pollutants. Elnour *et al*. reported a specific surface area of 249.13 m^2/g and a pore volume of 0.031 cm^3/g for biochar produced at 700 °C, providing a valuable context for understanding the characteristics of biochar across different production conditions.[67] Compared to the results from the current study, which demonstrate a higher specific surface area of 261.2 m^2/g for JS biochar at 600 °C. It suggests that the calcination temperature and feedstock type significantly influence the structural properties of biochar.[67] The higher surface area and potentially enhanced porosity of JS biochar may contribute to its superior adsorption capacity, making it a more effective adsorbent for contaminants such as ciprofloxacin and lamivudine. Additionally, these comparative results emphasize the importance of optimizing calcination conditions to maximize the adsorption potential of biochar, reinforcing the need for further studies to explore the relationship between production parameters and biochar properties in environmental applications. Muzyka *et al*.[68] reports a notably high surface area of 400 m^2/g and an average pore size of approximately 2.34 nm for biochar produced at 700 °C, and highlights the potential for optimizing biochar properties through precise control of production parameters. Compared to the surface area of 261.2 m^2/g reported in the current study for JS biochar calcined at 600 °C, which indicates that higher calcination temperatures can further improve the adsorptive capabilities of biochar. This emphasizes the importance of exploring various production conditions to maximize the efficiency of biochar as an adsorbent. Furthermore, the results contribute to the growing body of knowledge regarding biochar optimization for environmental applications, particularly in wastewater treatment and the removal of contaminants, reinforcing the need for continued research in this area. On the other hand, biochar made at a temperature below 400 °C had a lower surface area and pore volume. The current work presents surface areas of biochar calcined at 400 to 750 °C, and a relatively similar higher surface area and volume are observed, indicating similar results to previous studies.

3.3 Surface properties of adsorbent

Functional groups are critical surface properties of adsorbents that play a significant role in determining their adsorption capabilities and interactions with various adsorbates. Based on the analysis, a broad band at around 2900 to 3750 cm^{-1} in FTIR of JS biochar calcined at 500 °C indicates the presence of acidic (OH^-) hydroxyl groups, and a band at 1400 to 1850 cm^-

[1] corresponds to (C-O) stretching. Whereas, for JS biochar calcined at 400, 600, and 750 °C, a broad band at 3400 to 3850 cm^{-1} corresponds to (OH^-) hydroxyl groups, a band at 1600 to 2850 cm^{-1} corresponds to (C=O) stretching, a band at 1000 to 1350 cm^{-1} corresponds to (C-O) stretching, and 2950 to 3400 cm^{-1} may be due to C-H stretching (symmetrical for aliphatic and asymmetrical). The FTIR spectra of JS biochar calcined at 400, 600, and 750 °C are relatively similar and slightly different from the JS biochar calcined at 500 °C as presented in Fig. 5.

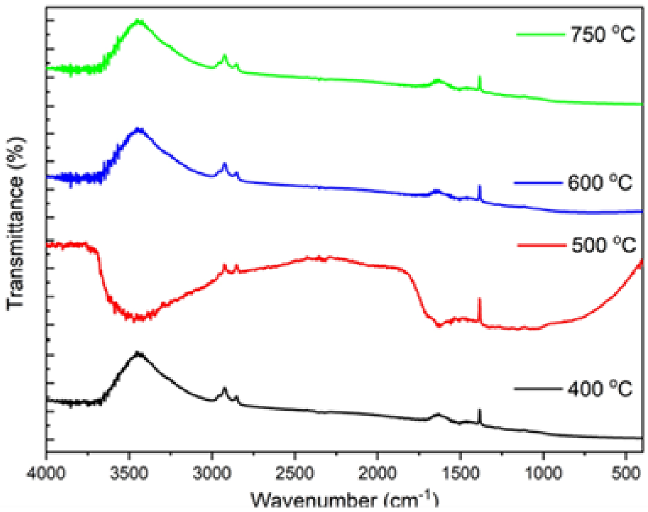

Fig. 5: FTIR spectra of JS biochar calcined at 400, 500, 600, and 750 °C, showing available functional groups potential for adsorption.

The FTIR spectra of JS biochar adsorbents calcined at various temperatures provide information on functional groups available that are potential for the adsorption ability of the material, Fig. 5. During calcination, the material undergoes various thermal transformations, including dehydration and the breakdown of organic components. This process can lead to the formation of hydroxyl groups (-OH) on the surface of the material. The loss of moisture and volatile compounds contributes to changes in the vibrational characteristics of these hydroxyl groups, resulting in specific stretching vibrations observed in FTIR spectra, as reported by other researchers.[61,69] These results indicate the surface of JS biochar is enriched with oxygen-containing groups and aromatic structures, which are necessary for the adsorption of contaminants, including ciprofloxacin, lamivudine, and inorganic pollutants.

A similar observation was reported by Fang *et al*., in their study, zeta potential curves were used to track the dissociation of these oxygen-containing surface groups. This indicated that when the pH increased, the H-bond donors on the biochar surface for ClO_4^- binding changed from -(COOH (ClO_4)$^-$···HOOC)- and -(OH (ClO_4-HO)-) to -OH alone.[70] Since high-temperature biochar provided a hydrophobic microenvironment to accommodate weakly hydrated perchlorate and facilitated the H-bonds for ClO_4^- binding to functional groups by their aromatic substrate's large π subunit, the H-bond force was strengthened by the condensed aromatic surfaces. This indicates that the interaction between biochar and perchlorate is highly dependent on the surface functional groups and environmental conditions, which has significant implications for the material's application in pollution mitigation.

The FTIR spectrum of JS biochar after ciprofloxacin adsorption shows that the peaks shifted from the initial position, as presented in Fig. 5. After ciprofloxacin adsorption, a new peak appeared at 2920 to 3800 cm^{-1} on the used adsorbent, which is like the peak observed in ciprofloxacin, and the peak intensity observed at 2920 to 3800 cm^{-1}. This result indicates that ciprofloxacin is adsorbed onto the surface of JS biochar through interactions with available functional groups (Fig. 6).

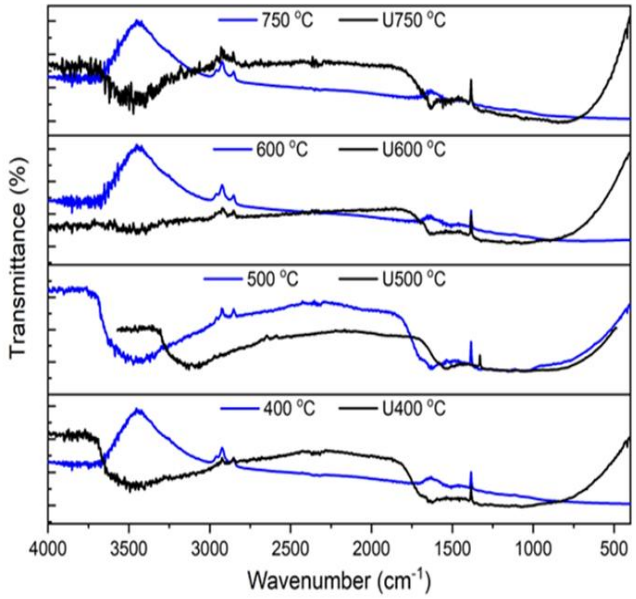

Fig. 6: Comparison of FTIR spectra of JS biochar used for adsorption of ciprofloxacin (Black) and unused (Blue)

The coexistence of different adsorption mechanisms highlights the complexity of the adsorption process and the importance of considering various interactions and factors when studying and utilizing adsorbents. It was observed for the adsorption of organics onto the JS biochar calcined at 600 °C, another mechanism was dominant. Hence, apart from the variations of surface properties for JS, biochar calcined at 750 °C had a relatively higher effectiveness. Further, the effectiveness of adsorbents calcined at 400 °C and 500 °C were relatively similar.

Similarly, for lamivudine adsorption Fig. 7, results show that after adsorption onto JS biochar, the peaks shifted from 3450 to 3400 cm^{-1}. A slight shift in peak position indicates that lamivudine adsorption onto JS biochar calcined at 400, 500, and 750 °C was through interactions with surface functional groups, leading to the appearance of peaks due to functional groups present.

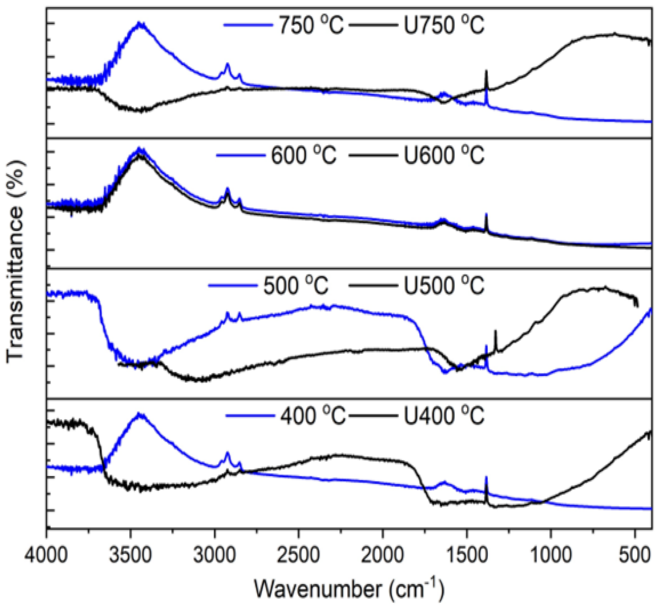

Fig. 7: Comparison of FTIR spectra of JS biochar used for adsorption of Lamivudine (Black) and unused (Blue).

This analysis indicates that the functional groups present in JS biochar calcined at various temperatures were involved in the adsorption process. This was observed for the adsorption of lamivudine onto JS biochar calcined at 600 °C. The variations of surface properties resulted in other mechanisms being dominant, such as pore-filling mechanisms, which is named as a limiting step. Previous researchers reported that the available functional groups on JS biochar played a significant role in adsorption utilizing electrostatic interactions, complexation, Pi-Pi interactions, and hydrogen bonding,[61,71] as observed in the recent study.[48]

3.4 Surface morphology

The surface morphology characterization by TEM involves detailed imaging of a material external structure at the nanoscale. This powerful technique utilizes a beam of transmitted electrons to provide high-resolution images, revealing surface features such as particles, pores, and crystalline structures. Fig. 8 presents TEM images of JS biochar prepared at 500 °C, (a) 500 nm image, (b) 100 nm image, (c) 1 µm image clearly showing the porous having rough surface, (d) 2 µm image, (e and g) a 50 nm images from varying orientations, (f) a 20 nm images showing the amorphic grains, and (h) a selected area electron diffraction (SAED) of an amorphous material revealing the characteristic halo ring patterns.

The TEM allows researchers to explore the intricate details of a material's topography, providing essential insights into its physical properties. From nanoparticles to biological specimens, TEM is instrumental in studying surface morphology, contributing to the advancements in materials science, nanotechnology, and the understanding of biological structures at the molecular level. Results of 2D TEM images (Figs. 8-10) present surface properties of JS biochar. The images indicate that JS biochar is a porous amorphous solid. Previous researchers reported similar results that the structure of biochar is largely amorphous but contains some local crystalline structure of highly conjugated aromatic compounds.[72,73]

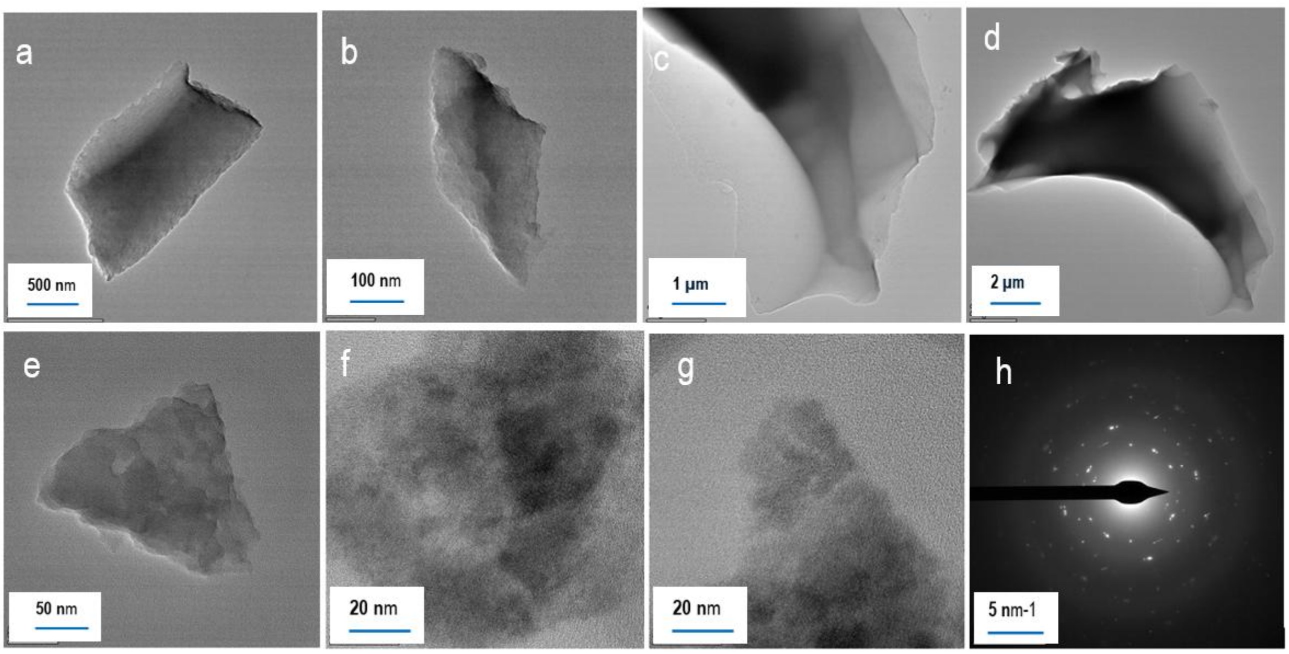

Fig. 8: The TEM images of JS biochar prepared at 500 °C, (a) 500 nm image, (b) 100 nm image, (c) 1 µm image clearly showing the porous having rough surface, (d) 2 µm image, (e) a 50 nm images from varying orientations, (f and g) 20 nm images showing the amorphic grains, and (h) a selected area electron diffraction (SAED) of an amorphous material revealing the characteristic halo ring patterns

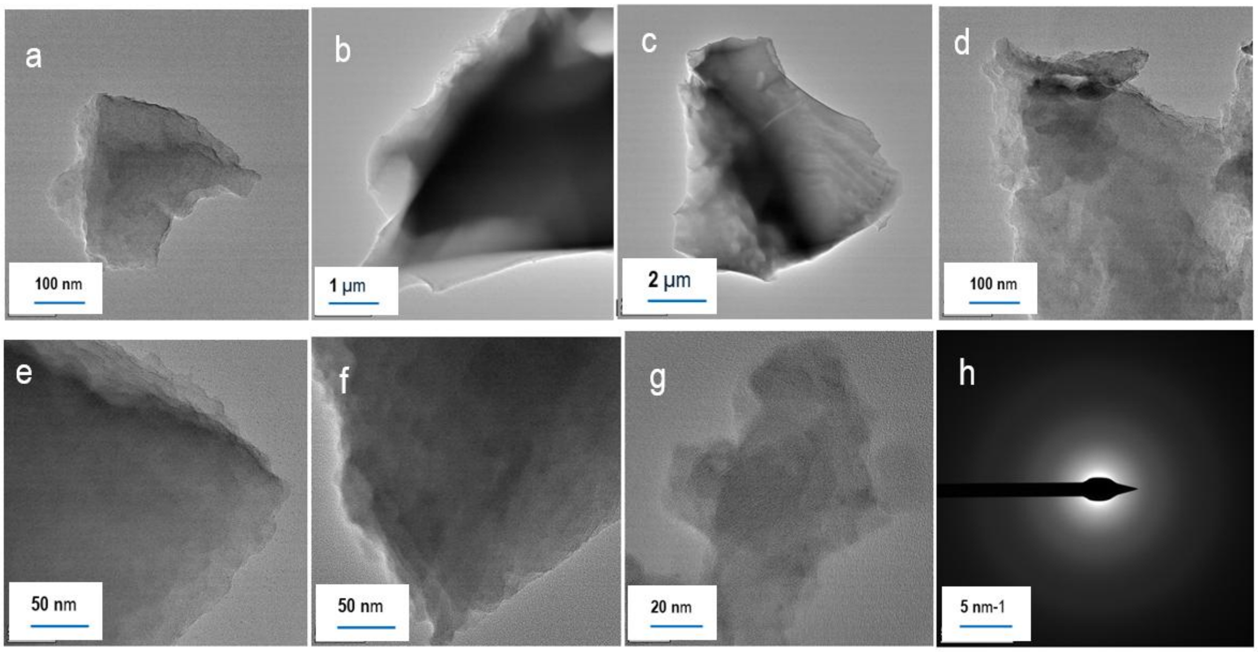

Fig. 9: The TEM images of Jamun seed biochar prepared at 600 °C, (a and d) 100 nm images from various orientations showing rough surface of the material, (b) 1 nm image, and (c) 2 nm image clearly showing the porous having rough surface, (e and g) 50 nm images from varying orientations, (f) a 20 nm image showing the amorphic grains, and (h) SAED of an amorphous material revealing the characteristic halo ring pattern.

The TEM images of jamun seed biochar prepared at 600 °C, (a and d) a 100 nm image from various orientations showing rough surface of the material, (b) 1 nm image, and (c) 2 nm images clearly showing the porous having rough surface, (e and g) a 50 nm images from varying orientations, (f) a 20 nm images showing the amorphic grains, and (h) SAED of an amorphous material revealing the characteristic halo ring pattern as presented in Fig. 9.

The TEM images of jamun seed biochar at 750 °C, are presented as follows: (a) a 500 nm, (b and e) a 100 nm from different orientations, (c) a 2 nm, and (d) a 100 nm images all showcasing the porous and rough surface of the JS biochar material. Additionally, (g and f) 20 nm images from different orientations, highlighting the amorphic grains, and (h) SAED of an amorphous material, which reveals the characteristic halo ring pattern, as shown in Fig. 10.

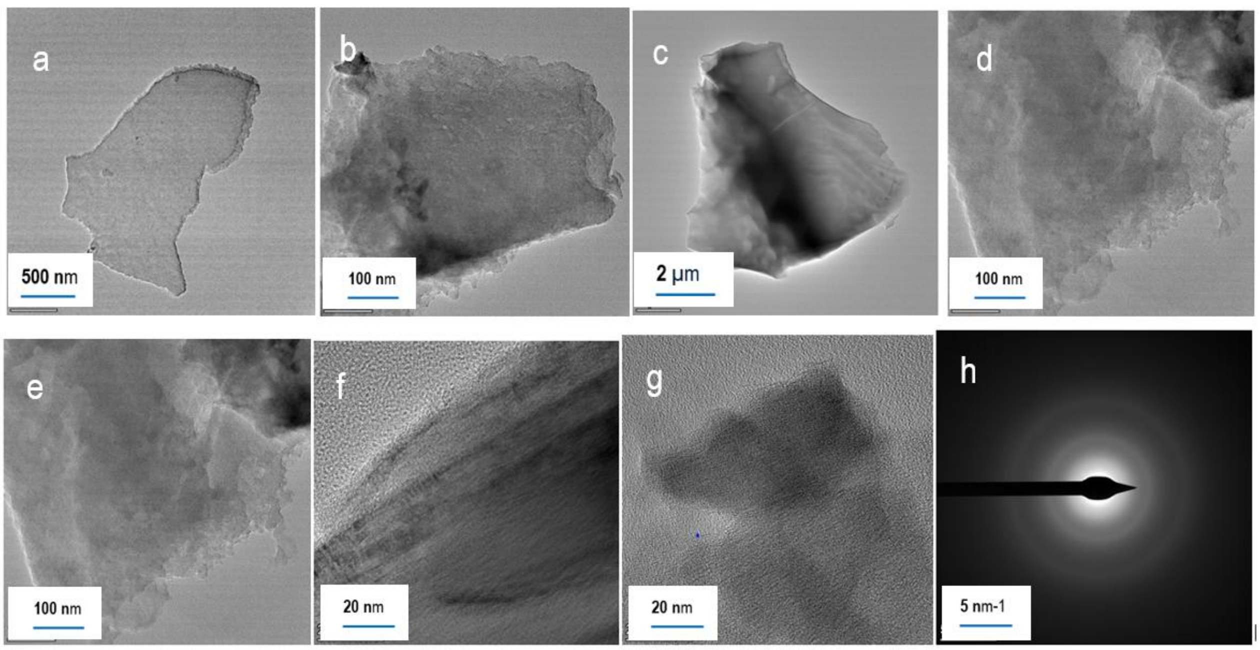

Fig. 10: The TEM images of Jamun seed biochar prepared at 750 °C, in various magnification and orientations and SAED image: (a) a 500 nm, (b and e) 100 nm from different orientations, (c) a 2 nm, and (d) a 100 nm images showing porous, rough surface of JS biochar material, (g and f) 20 nm images from different orientations, showing the amorphic grains, and (h) SAED of an amorphous material revealing the characteristic halo ring pattern.

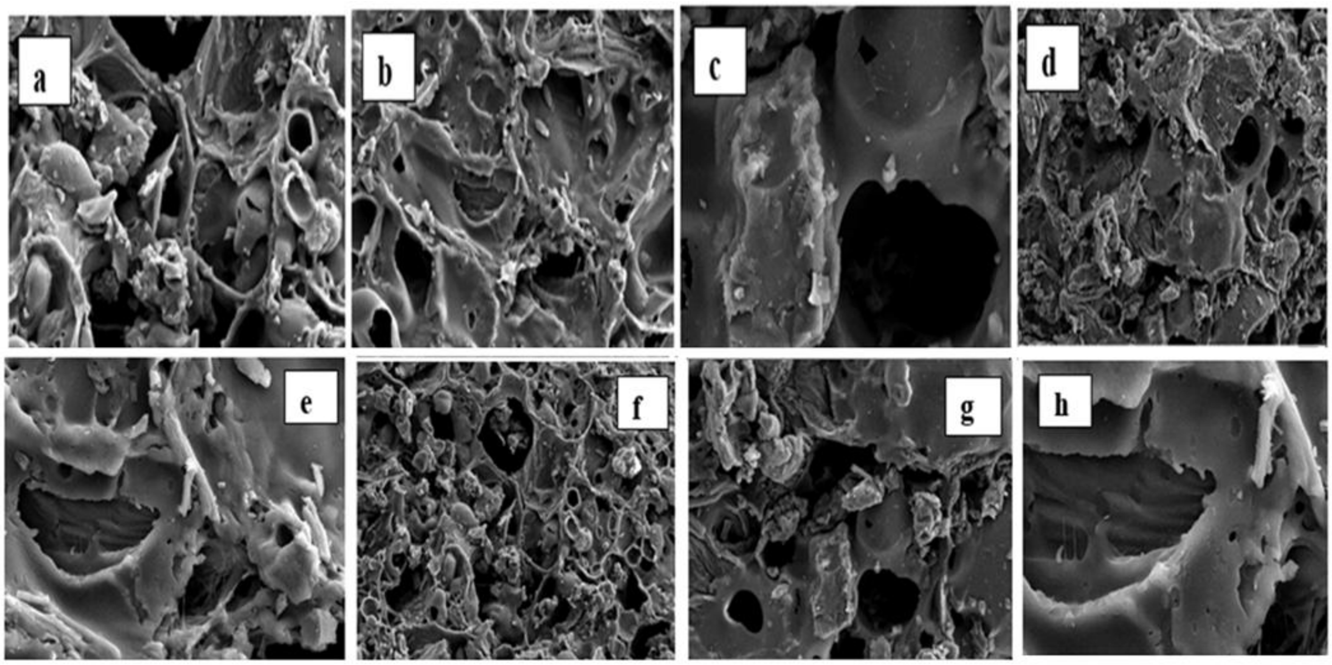

Fig. 11: The SEM images of unused JS biochar prepared at 600 °C, from various orientations, indicating porous nature and rough surface.

The results of the SEM analysis are presented in Figs. 11-13 show that JS biochar adsorbent possesses a rough mesoporous structure. Fig. 11 presents SEM images of unused JS biochar calcined at 600 °C from different orientations and magnifications. The images indicate that JS biochar adsorbent possesses porous, rough surface potential interactions with adsorbate, leading to adsorptive remediation.

Similarly, Fig. 12 presents SEM images for JS biochar prepared at 600 °C used for a single cycle of Lamivudine adsorption from various orientations, indicating that the adsorbent is not loaded and can be used for other cycles.

Fig. 13 presents SEM images for JS biochar prepared at 600 °C used for a single cycle of ciprofloxacin adsorption from various orientations, indicating that the adsorbent is not loaded and can be used for other cycles.

The composition distribution varies greatly from one biochar to another and is greatly influenced by the biochar precursor and the synthesis circumstances. Previous scholars

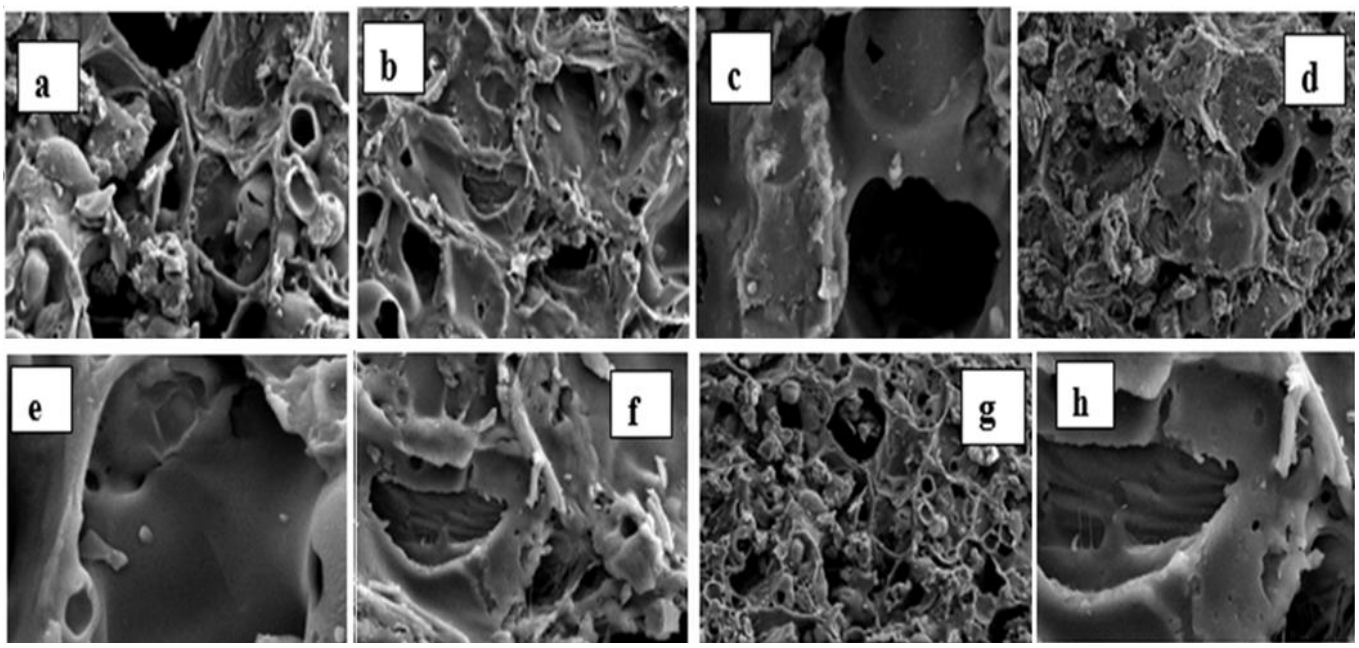

Fig. 12: The SEM images for JS biochar prepared at 600 °C and used for Lamivudine adsorption from various orientations, indicating porous nature and rough surface.

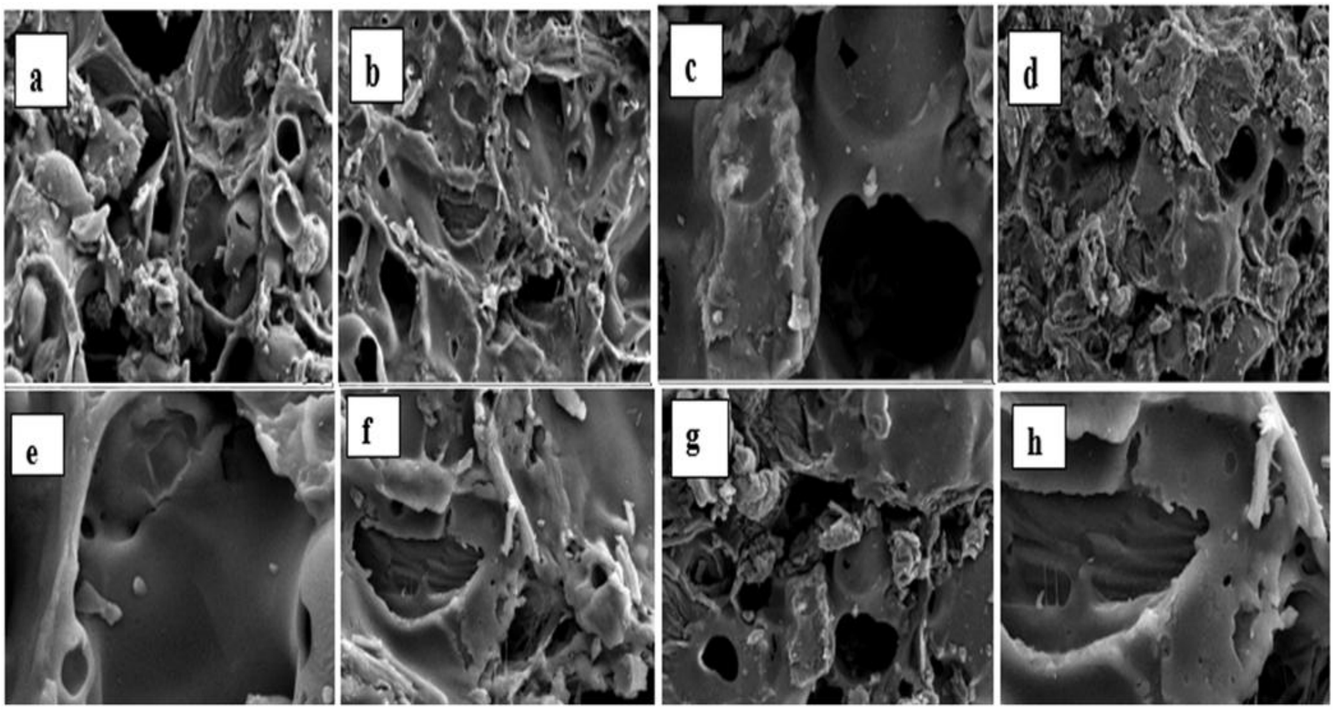

Fig. 13: The SEM images for JS biochar prepared at 600 °C and used for a single cycle of ciprofloxacin adsorption from various orientations, indicating the porous nature of the adsorbent and rough surface.

reported that most of the biochar contains carbon, oxygen, heteroatoms (such as N and S), and minerals (Na, C, and K),[74] as observed in this study, Fig. 14.

The results of the XRD analysis of JS biochar adsorbent are presented in Figs. 15-17, for the unused JS biochar calcined at 750 °C (Blue), calcined at 600 °C (Red) and calcined at 500 °C (Black). The observed diffraction peaks are due to the presence of functional groups on aromatic compounds. The presence of a surface functional group was initially verified by the results of FTIR analysis (Fig. 5). Its changes after adsorption of lamivudine (Fig. 6) and ciprofloxacin (Fig. 7). In the diffraction area of 20°-65° for biochar calcined at 750 °C, 30°-65° for biochar calcined at 600 °C, 40°-65° for biochar calcined at 500 °C, obvious diffraction peaks can be observed on the unused biochar samples, previous researchers reported similar trends.[75,76] The results of the XRD analysis of unused JS are presented in Fig. 15, which indicates the material is amorphous.

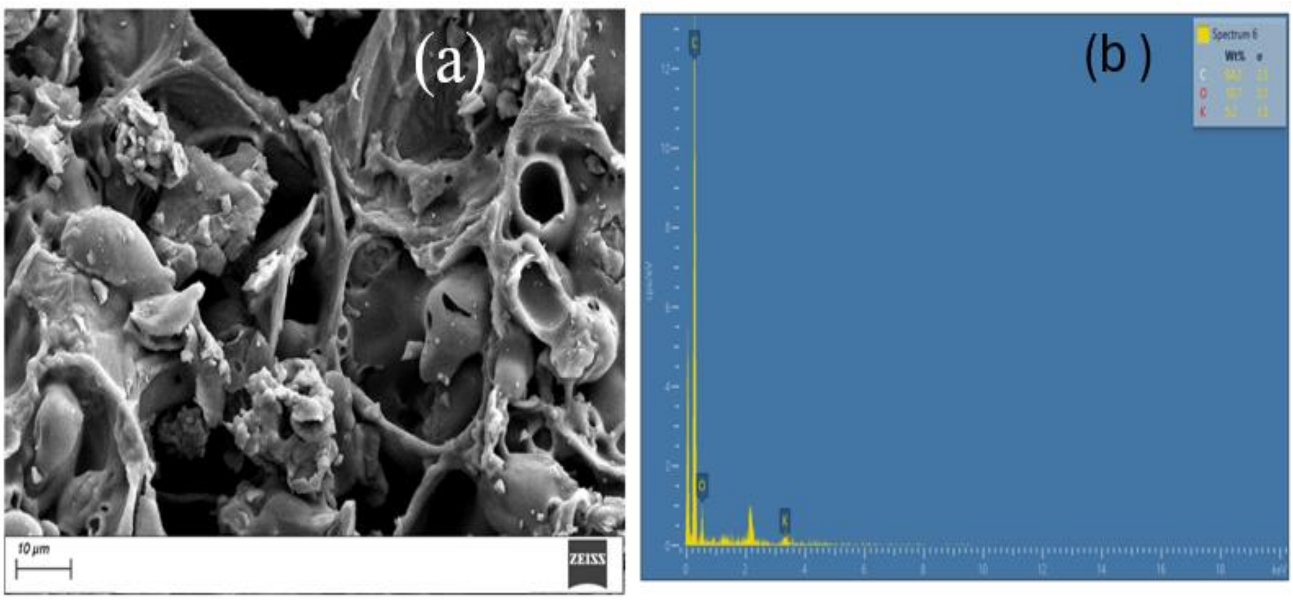

Fig. 14: SEM image (a) EDAX image of used JS biochar calcined at 600 °C showing the porous, rough surface of the adsorbent and (b) Elemental compositions of used JS biochar.

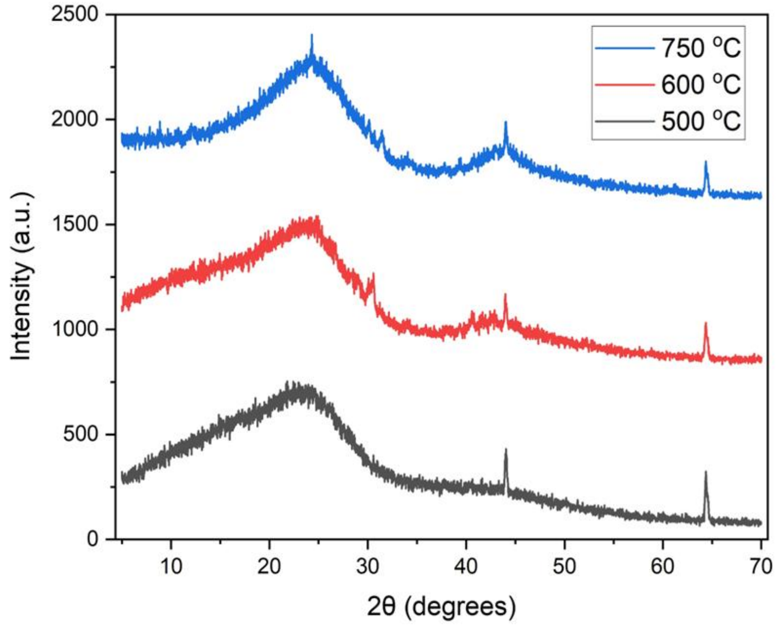

Fig. 15: The XRD results of unused JS biochar calcined at 750 °C (Blue), calcined at 600 °C (Red), and calcined at 500 °C (Black).

By comparing the peak changes before and after lamivudine adsorption, it was found that the peak strength was enhanced and shifted to 42.5°-65° for all adsorbents, indicating the presence of Lamivudine onto JS biochar adsorbents. Fig. 16 presents the comparison of the XRD results of unused JS biochar (Blue) used for the adsorption of Lamivudine (Black).

By comparing the peak changes before and after lamivudine adsorption, it was found that the peak strength was enhanced and shifted to 45°-65° for all adsorbents, indicating the presence of ciprofloxacin onto JS biochar adsorbents. Fig. 17 presents the comparison of the XRD results of unused JS biochar (Blue) used for adsorption of ciprofloxacin (Black).

Adsorbent properties are intrinsic qualities of materials, enabling them to accumulate molecules or particles on their surface. This process occurs due to attractive forces between the JS biochar and the adsorbate, such as Lamivudine and ciprofloxacin.[77] The adsorptive removal of contaminants such as Lamivudine and ciprofloxacin onto adsorbent such as JS biochar depends on the properties of the adsorbent, including specific surface area, porosity, and chemical composition. Similarly, the carbon content of biochar typically ranges from 50% to 95%, depending on the feedstock and pyrolysis conditions,[78] as similarly observed in the current study. Functional groups play a significant role in adsorption processes by influencing the interactions between adsorbents

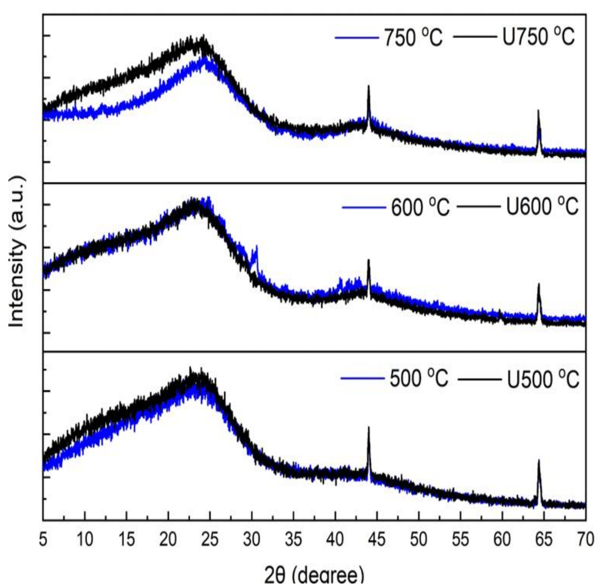

Fig. 16: Comparison of the XRD results of unused JS biochar (Blue) used for adsorption of Lamivudine (Black).

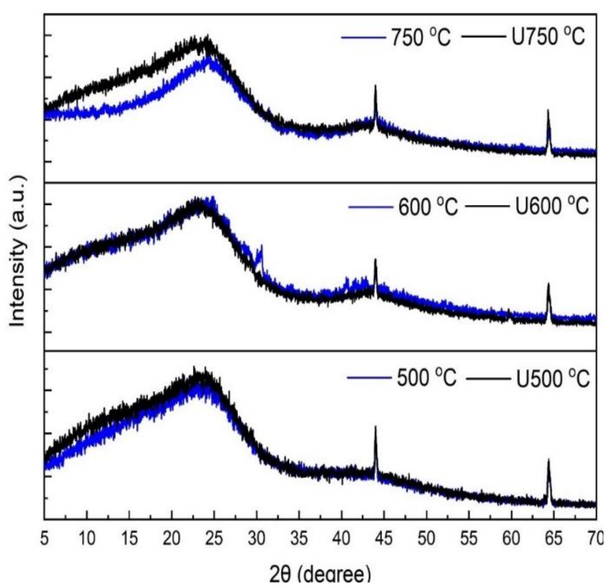

Fig. 17: Comparison of the XRD results of unused JS biochar (Blue) used for adsorption of Ciprofloxacin (Black).

and adsorbates. These groups, such as hydroxyl (-OH), carboxyl (-COOH), amino ($-NH_2$),[79] and others, introduce specific chemical properties to the surface of materials.

The presence of functional groups enhances adsorption through hydrogen bonding, electrostatic interactions, and van der Waals forces. Surface area is a critical factor in adsorption processes.[80] Adsorption occurs on the surface of a material, and a larger surface area provides more sites for adsorbate molecules to interact and adhere. Materials with a high specific surface area are highly effective adsorbents due to their numerous available binding sites. Pore size significantly influences adsorption processes. Adsorbents with well-defined pore structures, including different pore sizes like micropores, mesopores, and macropores, offer distinct adsorption capabilities.

Similarly, pore volume is a crucial parameter in adsorption processes, determining the amount of adsorbate that can be accommodated within an adsorbent material.[80] It refers to the total volume of empty spaces or pores within the material that can trap and retain molecules. Materials with higher pore volume can hold more adsorbate molecules, leading to greater adsorption capacities. In a similar manner, surface morphology significantly impacts adsorption processes. The physical characteristics of an adsorbent's surface, including roughness, porosity, and structure, influence its interactions with adsorbate molecules. A rough or textured surface provides more sites for adsorption to occur due to increased surface area. Porous structures, like those found in activated carbon or zeolites, enhance adsorption by offering multiple binding sites within the pores. Surface irregularities and features can also create microenvironments that favor specific interactions, such as hydrogen bonding or van der Waals forces.

Further, the adsorption process may occur through physical processes (physisorption) or chemical processes (chemisorption). Physisorption occurs due to weak van der Waals forces between the adsorbent and adsorbate molecules. It is a reversible process where molecules are attracted to the surface through intermolecular forces, such as London dispersion forces, dipole-dipole interactions, and hydrogen bonding, and influenced by factors like temperature, pressure, and the surface area of the adsorbent. On the other hand, chemisorption involves stronger chemical bonds forming between the adsorbent and adsorbate molecules. This can include covalent bonds or ionic interactions. It's usually a more specific and irreversible process, often requires activation energy, and may involve surface functional groups or active sites on the adsorbent. These processes can coexist depending on the nature of the adsorbate and the adsorbent surface. The choice between these mechanisms depends on factors such as the nature of the materials, temperature, pressure, and the presence of other substances. Understanding the mechanism of adsorption is crucial in various applications, including purification, separation, catalysis, and environmental remediation. It determines the effectiveness of adsorbent materials and aids in designing optimized processes for specific adsorption needs.

4. Conclusion

The analysis of JS biochar reveals several significant findings regarding its characteristics and performance as an adsorbent. Increasing the calcination temperature from 400 to 600 °C results in a notable rise in carbon and nitrogen content, enhancing its adsorption capabilities. However, temperatures exceeding 700 °C lead to a decrease in carbon content, likely due to the removal of ligands and organic matter. The biochar exhibits impressive surface properties, with a peak surface area of 261.2 m^2/g, providing numerous active sites for adsorption, particularly for small antimicrobial molecules like ciprofloxacin (555.55 mg/g) and lamivudine (400 mg/g). Functional groups, such as hydroxyl and carbonyl, identified through FTIR analysis, play a crucial role in promoting interactions through hydrogen bonding, electrostatic interactions, and complexation with the adsorbates. Surface morphology studies using TEM and SEM demonstrate that the biochar possesses a rough mesoporous structure, which significantly enhances its adsorptive capacity. Furthermore, the data suggest that various adsorption mechanisms, including both physisorption and chemisorption, may coexist, indicating a complex interplay of weak and strong interactions during the adsorption process. Lastly, the sustainable sourcing of JS biochar from jamun seeds not only addresses waste management but also positions it as a viable solution for environmental remediation, effectively mitigating pollutants from water sources. Overall, the findings suggest that JS biochar is a highly effective adsorbent with a promising potential for applications in environmental cleanup.

Conflict of Interest

There is no conflict of interest.

Supporting Information

Not applicable.

References

[1] U. Anand, B. Reddy, V. K. Singh, A. K. Singh, K. K. Kesari, P. Tripathi, P. Kumar, V. Tripathi, J. Simal-Gandara, Potential environmental and human health risks caused by antibiotic-resistant bacteria (ARB), antibiotic resistance genes (ARGs) and emerging contaminants (ECs) from municipal solid waste (MSW) landfill, *Antibiotics*, 2021, **10**, 374, doi: 10.3390/antibiotics10040374.

[2] K. W. K. Tang, B. C. Millar, J. E. Moore, Antimicrobial resistance (AMR), *British Journal of Biomedical Science*, 2023, **80**, 11387, doi: 10.3389/bjbs.2023.11387.

[3] K. Amaratunga, J. Tarasuk, L. Tsegaye, C. P. Archibald, Advancing surveillance of antimicrobial resistance: summary of the 2015 CIDSC report, *Canada Communicable Disease Report*, 2016, **42**, 232-237, doi: 10.14745/ccdr.v42i11a03.

[4] A. S. Ripanda, M. J. Rwiza, E. C. Nyanza, H. Miraji, N. L.

Bih, A. Mzula, E. Mwega, K. N. Njau, S. Ali Hamad Vuai, R. L. Machunda, Antibiotic-resistant microbial populations in urban receiving waters and wastewaters from Tanzania, *Environmental Chemistry and Ecotoxicology*, 2023, **5**, 1-8, doi: 10.1016/j.enceco.2022.10.003.

[5] H. Miraji, A. Ripanda, E. Moto, A review on the occurrences of persistent organic pollutants in corals, sediments, fish and waters of the Western Indian Ocean, *Egyptian Journal of Aquatic Research*, 2021, **47**, 373-379, doi: 10.1016/j.ejar.2021.08.003.

[6] A. Ripanda, M. J. Rwiza, E. C. Nyanza, L. N. Bih, M. Hossein, R. Bakari, S. K. Sigh, G. Reddy, C. R. Ravikumar, H. C. Ananda Murthy, K. N. Njau, S. Ali Hamad Vuai, R. L. Machunda, Optimizing ciprofloxacin removal from water using jamun seed (Syzygium cumini) biochar: A sustainable approach for ecological protection, *HydroResearch*, 2024, **7**, 164-180, doi: 10.1016/j.hydres.2024.03.001.

[7] M. Hossein, Toxicological aspects of emerging contaminants, Emerging and Eco-Friendly Approaches for Waste Management, Singapore: Springer Singapore, 2019, 33-58, ISBN: 9789811086694.

[8] H. Miraji, O. C. Othman, F. Ngassapa, M. Eunice, Analytical perspectives on emerging organic contaminants in the aquatic ecosystem, Effects of Emerging Chemical Contaminants on Water Resources and Environmental Health, IGI GlobalPublish, 2020, 68-80, ISBN: 9781799818717.

[9] M. Hossein, R. Asha, R. Bakari, N. F. Islam, G. Jiang, H. Sarma, Exploring eco-friendly approaches for mitigating pharmaceutical and personal care products in aquatic ecosystems: A sustainability assessment, *Chemosphere*, 2023, **316**, 137715, doi: 10.1016/j.chemosphere.2022.137715.

[10] N. L. Bih, M. J. Rwiza, A. S. Ripanda, A. A. Mahamat, R. L. Machunda, J. W. Choi, Adsorption of phenol and methylene blue contaminants onto high-performance catalytic activated carbon from biomass residues, *Heliyon*, 2025, **11**, e41150, doi: 10.1016/j.heliyon.2024.e41150.

[11] A. Ripanda, M. Hossein, M. J. Rwiza, E. C. Nyanza, J. R. Selemani, S. Nkrumah, R. Bakari, M. S. Alfred, R. L. Machunda, S. Ali Hamad Vuai, Combatting toxic chemical elements pollution for Sub-Saharan Africa's ecological health, *Environmental Pollution and Management*, 2025, **2**, 42-62, doi: 10.1016/j.epm.2025.01.003.

[12] A. S. Ripanda, M. J. Rwiza, E. C. Nyanza, R. L. Machunda, S. H. Vuai, Contribution of illicit drug use to pharmaceutical load in the environment: a focus on sub-Saharan Africa, *Journal of Environmental and Public Health*, 2022, **2022**, 9056476, doi: 10.1155/2022/9056476.

[13] A. S. Ripanda, M. J. Rwiza, E. C. Nyanza, K. N. Njau, S. A. H. Vuai, R. L. Machunda, A review on contaminants of emerging concern in the environment: a focus on active chemicals in sub-Saharan Africa, *Applied Sciences*, 2022, **12**, 56, doi: 10.3390/app12010056.

[14] H. Miraji, M. Eunice, A. Ripanda, F. Ngassapa, O. Chande, Naturally occurring emerging contaminants: Where to hide?, *HydroResearch*, 2023, **6**, 203-215, doi: 10.1016/j.hydres.2023.05.002.

[15] R. H. Mdegela, E. R. Mwakapeje, B. Rubegwa, D. T. Gebeyehu, S. Niyigena, V. Msambichaka, H. E. Nonga, N. Antoine-Moussiaux, F. O. Fasina, Antimicrobial use, residues, resistance and governance in the food and agriculture sectors, Tanzania, *Antibiotics*, 2021, **10**, 454, doi: 10.3390/antibiotics10040454.

[16] C. L. Moo, S. K. Yang, K. Yusoff, M. Ajat, W. Thomas, A. Abushelaibi, S. H. E. Lim, K. S. Lai, Mechanisms of antimicrobial resistance (AMR) and alternative approaches to overcome AMR, *Current Drug Discovery Technologies*, 2020, **17**, 430-447, doi: 10.2174/1570163816666190304122219.

[17] R. Bakari, R. Asha, M. Hossein, X. Huang, N. F. Islam, R. K. Liew, M. Narayan, S. S. Lam, H. Sarma, Converting food waste to biofuel: a sustainable energy solution for sub-Saharan Africa, *Sustainable Chemistry for the Environment*, 2024, **7**, 100126, doi: 10.1016/j.scenv.2024.100126.

[18] F. Baquero, Threats of antibiotic resistance: an obliged reappraisal, *International Microbiology*, 2021, **24**, 499-506, doi: 10.1007/s10123-021-00184-y.

[19] A. Talebi Bezmin Abadi, A. A. Rizvanov, T. Haertlé, N. L. Blatt, World health organization report: current crisis of antibiotic resistance, *BioNanoScience*, 2019, **9**, 778-788, doi: 10.1007/s12668-019-00658-4.

[20] S. S. Kadri, Key takeaways from the U.S. CDC's 2019 antibiotic resistance threats report for frontline providers, *Critical Care Medicine*, 2020, **48**, 939-945, doi: 10.1097/ccm.0000000000004371.

[21] C. Seiler, T. U. Berendonk, Heavy metal driven co-selection of antibiotic resistance in soil and water bodies impacted by agriculture and aquaculture, *Frontiers in Microbiology*, 2012, **3**, 399, doi: 10.3389/fmicb.2012.00399.

[22] A. Ripanda, M. J. Rwiza, E. C. Nyanza, M. Hossein, M. S. Alfred, A. El-Din Mahmoud, H. C. A. Murthy, R. Bakari, S. Ali Hamad Vuai, R. L. Machunda, Ecological consequences of antibiotics pollution in sub-Saharan Africa: Understanding sources, pathways, and potential implications, *Emerging Contaminants*, 2025, **11**, 100475, doi: 10.1016/j.emcon.2025.100475.

[23] A. N. Siyal, S. Q. Memon, M. Amanullah, T. Pirzada, S. Parveen, N. A. Sodho, Multi-variant sorption optimization for the uptake of Pb(II) ions by jamun seed waste, *Polish Journal of Chemical Technology*, 2013, **15**, 15-21, doi: 10.2478/pjct-2013-0004.

[24] R. Araga, S. Soni, C. S. Sharma, Fluoride adsorption from aqueous solution using activated carbon obtained from KOH-treated jamun (Syzygium cumini) seed, *Journal of Environmental Chemical Engineering*, 2017, **5**, 5608-5616, doi: 10.1016/j.jece.2017.10.023.

[25] S. Deka, K. G. Bhattacharyya, Column studies on chromium (VI) adsorption onto kala jamun (syzygiumcumini L.) seed powder (KSP), *International Journal of Advances in Chemical Engineering and Biological Sciences*, 2017, **4**, 93-97, doi: 10.15242/ijacebs.a0217017.

[26] J. Shah, I. Sharma, O. Silakari, R. Sharma, Removal of

As (III) ion using Syzygium cumini seeds (SCS) biomass from ground water and waste water, *International Journal of Engineering and Applied Sciences*, 2017, **4**, 257379.

[27] A. Nilavazhagi, T. Felixkala, Adsorptive removal of Fe(II) ions from water using carbon derived from thermal/chemical treatment of agricultural waste biomass: Application in groundwater contamination, *Chemosphere*, 2021, **282**, 131060, doi: 10.1016/j.chemosphere.2021.131060.

[28] D. Kosale, C. Thakur, V. K. Singh, Utilization of Jamun seed (Syzyum Cumini) biochar for removal of Fuchsin dye from aqueous solution, *Journal of the Serbian Chemical Society*, 2023, **88**, 653-667, doi: 10.2298/JSC220830021K.

[29] A. Ripanda, M. J. Rwiza, E. C. Nyanza, R. Bakari, H. Miraji, K. N. Njau, S. Ali Hamad Vuai, R. L. Machunda, Data from the batch adsorption of ciprofloxacin and lamivudine from synthetic solution using jamun seed (Syzygium cumini) biochar: Response surface methodology (RSM) optimization, *Data in Brief*, 2023, **47**, 108975, doi: 10.1016/j.dib.2023.108975.

[30] A. Ripanda, M. J. Rwiza, E. C. Nyanza, R. Bakari, H. Miraji, K. N. Njau, S. Ali Hamad Vuai, R. L. Machunda, Removal of lamivudine from synthetic solution using jamun seed (Syzygium cumini) biochar adsorbent, *Emerging Contaminants*, 2023, **9**, 100232, doi: 10.1016/j.emcon.2023.100232.

[31] M. Qamar, S. Akhtar, T. Ismail, M. Wahid, M. W. Abbas, M. S. Mubarak, Y. Yuan, R. T. Barnard, Z. M. Ziora, T. Esatbeyoglu, Phytochemical profile, biological properties, and food applications of the medicinal plant syzygium cumini, *Foods*, 2022, **11**, 378, doi: 10.3390/foods11030378.

[32] U. Prajapati, V. Ksh, A. Joshi, Extraction and use of bioactive components from underutilized horticultural crops, Bioactive Components, Singapore: Springer Nature Singapore, 2022, 535-570, ISBN: 978-981-19-2365-4.

[33] J. Prakash, A. Maurya, S. Singh, Studies on variability in fruit characters of jamun, *Indian Journal of Horticulture*, 2010, **67**, 63-66.

[34] C. Liu, P. Luan, Q. Li, Z. Cheng, P. Xiang, D. Liu, Y. Hou, Y. Yang, H. Zhu, Biopolymers derived from trees as sustainable multifunctional materials: a review, *Advanced Materials*, 2021, **33**, 2001654, doi: 10.1002/adma.202001654.

[35] N. Mabungela, N. D. Shooto, F. Mtunzi, E. B. Naidoo, The adsorption of copper, lead metal ions, and methylene blue dye from aqueous solution by pure and treated fennel seeds, *Adsorption Science & Technology*, 2022, **2022**, 5787690, doi: 10.1155/2022/5787690.

[36] A. G. Choudhury, P. Roy, S. Kumari, V. K. Singh, Utility of fruit-based industry waste, Handbook of Solid Waste Management. Singapore: Springer Nature Singapore, 2022, 757-784, ISBN: 9789811575259.

[37] A. Komesu, L. H. da Silva Martins, P. Pandey, A. Kuila, C. F. A. Penteado, E. D. Penteado, J. A. R. de Oliveira, Fruit and vegetable waste an economic alternate to costlier raw materials for value added products, Waste Management, Boca Raton: CRC Press, 2022, 60-82, ISBN: 9780429341106.

[38] C. F. Varela, L. C. Moreno-Aldana, Y. Y. Agámez-Pertuz, Adsorption of pharmaceutical pollutants on $ZnCl_2$-activated biochar from corn cob: Efficiency, selectivity and mechanism, *Journal of Bioresources and Bioproducts*, 2024, **9**, 58-73, doi: 10.1016/j.jobab.2023.10.003.

[39] S. B. Daffalla, H. Mukhtar, M. S. Shaharun, Preparation and characterization of rice husk adsorbents for phenol removal from aqueous systems, *PLoS One*, 2020, **15**, e0243540, doi: 10.1371/journal.pone.0243540.

[40] Y. Li, B. Xing, X. Wang, K. Wang, L. Zhu, S. Wang, Nitrogen-doped hierarchical porous biochar derived from corn stalks for phenol-enhanced adsorption, *Energy & Fuels*, 2019, **33**, 12459-12468, doi: 10.1021/acs.energyfuels.9b02924.

[41] A. C. Martins, O. Pezoti, A. L. Cazetta, K. C. Bedin, D. A. S. Yamazaki, G. F. G. Bandoch, T. Asefa, J. V. Visentainer, V. C. Almeida, Removal of tetracycline by NaOH-activated carbon produced from macadamia nut shells: Kinetic and equilibrium studies, *Chemical Engineering Journal*, 2015, **260**, 291-299, doi: 10.1016/j.cej.2014.09.017.

[42] M. A. Al Masud, S. Annamalai, W. S. Shin, Remediation of ciprofloxacin in soil using peroxymonosulfate activated by ball-milled seaweed kelp biochar: Performance, mechanism, and phytotoxicity, *Chemical Engineering Journal*, 2023, **465**, 142908, doi: 10.1016/j.cej.2023.142908.

[43] J. Ouyang, J. Chen, W. Chen, L. Zhou, D. Cai, C. Ren, H_3PO_4 activated biochars derived from different agricultural biomasses for the removal of ciprofloxacin from aqueous solution, *Particuology*, 2023, **75**, 217-227, doi: 10.1016/j.partic.2022.07.016.

[44] Ç. Özer, M. İmamoğlu, Removal of ciprofloxacin from aqueous solutions by pumpkin peel biochar prepared using phosphoric acid, *Biomass Conversion and Biorefinery*, 2024, **14**, 6521-6531, doi: 10.1007/s13399-022-02832-3.

[45] L. Azeez, O. Adefunke, A. O. Oyedeji, B. K. Agbaogun, H. K. Busari, A. L. Adejumo, W. B. Agbaje, A. E. Adeleke, A. O. Samuel, Facile removal of rhodamine B and metronidazole with mesoporous biochar prepared from palm tree biomass: adsorption studies, reusability, and mechanisms, *Water Practice & Technology*, 2024, **19**, 730-744, doi: 10.2166/wpt.2024.049.

[46] E. J. Mumba, J. S. Rajabu, H. R. Kasambala, A. Ripanda, J. M. Bidu, M. Rwiza, Data on preliminary dust exposure assessment, its composition, and health implications for workers in the artisanal and small-scale Tanzanite mining industry in Mererani, Tanzania, doi: 10.1080/03067319.2024.2448546.

[47] A. R. Ripanda, Data on Jamun Seed (Syzygium cumini) Biochar, surface properties, and adsorption of Ciprofloxacin and Lamivudine: Part 2, doi: 10.17632/2bkk7rxntv.1.

[48] A. Ripanda, Emerging pollution, antimicrobial resistance, and the applicability of biochar adsorbents: A comprehensive study in African water systems, The Nelson Mandela African Institution of Science and Technology, PhD, NM-AIST, 2024, doi: 10.58694/20.500.12479/2730.

[49] C. A. Igwegbe, S. N. Oba, C. O. Aniagor, A. G. Adeniyi,

J. O. Ighalo, Adsorption of ciprofloxacin from water: a comprehensive review, *Journal of Industrial and Engineering Chemistry*, 2021, **93**, 57-77, doi: 10.1016/j.jiec.2020.09.023.

[50] J. Ma, M. Yang, F. Yu, J. Zheng, Water-enhanced removal of ciprofloxacin from water by porous graphene hydrogel, *Scientific Reports*, 2015, **5**, 13578, doi: 10.1038/srep13578.

[51] S. Dou, X. Ke, Z. Shao, L. Zhong, Q. Zhao, Y. Zheng, Fish scale-based biochar with defined pore size and ultrahigh specific surface area for highly efficient adsorption of ciprofloxacin, *Chemosphere*, 2022, **287**, 131962, doi: 10.1016/j.chemosphere.2021.131962.

[52] J. Späth, P. Arumugam, R. H. Lindberg, O. A. Abafe, S. Jansson, J. Fick, C. A. Buckley, Biochar for the removal of detected micropollutants in South African domestic wastewater: a case study from a demonstration-scale decentralised wastewater treatment system in eThekwini, *Water SA*, 2021, **47**, 396-416.

[53] F. Qin, C. Zhang, G. Zeng, D. Huang, X. Tan, A. Duan, Lignocellulosic biomass carbonization for biochar production and characterization of biochar reactivity, *Renewable and Sustainable Energy Reviews*, 2022, **157**, 112056, doi: 10.1016/j.rser.2021.112056.

[54] M. J. Anderson, P. J. Whitcomb, RSM simplified: optimizing processes using response surface methods for design of experiments, Productivity press, 2016, ISBN: 9781498745987.

[55] X. Jiang, S. Zhang, X. Yin, Y. Tian, Y. Liu, Z. Deng, L. Wang, Contrasting effects of a novel biochar-microalgae complex on arsenic and mercury removal, *Ecotoxicology and Environmental Safety*, 2023, **262**, 115144, doi: 10.1016/j.ecoenv.2023.115144.

[56] M. Chen, X. Chen, X. Xu, Z. Xu, Y. Zhang, B. Song, D. C. W. Tsang, N. Xu, X. Cao, Biochar colloids facilitate transport and transformation of Cr(VI) in soil: Active site competition coupling with reduction reaction, *Journal of Hazardous Materials*, 2022, **440**, 129691, doi: 10.1016/j.jhazmat.2022.129691.

[57] S. Sert, Ş. S. Gültekin, D. D. Kaya, A. Körlü, Development of activated carbon from hemp hurd for EMI shielding and supercapacitors *via* one-step microwave pyrolysis without inert gas, *Biomass Conversion and Biorefinery*, 2024, 1-20, doi: 10.1007/s13399-024-06330-6.

[58] Z. Xuan, L. Gurevich, J. de Claville Christiansen, V. Zachar, C. P. Pennisi, Stable hydrogel adhesion to polydimethylsiloxane enables cyclic mechanical stimulation of 3D-bioprinted smooth muscle constructs, *Biotechnology and Bioengineering*, 2023, **120**, 3396-3408, doi: 10.1002/bit.28516.

[59] A. Ripanda, M. Rwiza, E. Nyanza, R. Bakari, H. Miraji, S. Vuai, K. Njau, R. Machunda, Data on jamun seed (syzygium cumini) biochar; preparation, initial characterization, experimental design and adsorption of ciprofloxacin and lamivudine: Part 1, Mendeley Data, 2022, doi: 10.17632/pphv3ygkfk.1.

[60] R. Ojeda-López, G. Ramos-Sánchez, C. García-Mendoza, D. C. S. Azevedo, A. Guzmán-Vargas, C. Felipe, Effect of calcination temperature and chemical composition of PAN-derived carbon microfibers on N_2, CO_2, and CH_4 adsorption, *Materials*, 2021, **14**, 3914, doi: 10.3390/ma14143914.

[61] S. Wang, J. Wang, Nitrogen doping sludge-derived biochar to activate peroxymonosulfate for degradation of sulfamethoxazole: Modulation of degradation mechanism by calcination temperature, *Journal of Hazardous Materials*, 2021, **418**, 126309, doi: 10.1016/j.jhazmat.2021.126309.

[62] M. Liu, E. Almatrafi, Y. Zhang, P. Xu, B. Song, C. Zhou, G. Zeng, Y. Zhu, A critical review of biochar-based materials for the remediation of heavy metal contaminated environment: Applications and practical evaluations, *Science of the Total Environment*, 2022, **806**, 150531, doi: 10.1016/j.scitotenv.2021.150531.

[63] W. Liu, H. Jiang, H. Yu, Development of biochar-based functional materials: toward a sustainable platform carbon material, *Chemical Reviews*, 2015, **115**, 12251-12285, doi: 10.1021/acs.chemrev.5b00195.

[64] G. Leofanti, M. Padovan, G. Tozzola, B. Venturelli, Surface area and pore texture of catalysts, *Catalysis Today*, 1998, **41**, 207-219, doi: 10.1016/S0920-5861(98)00050-9.

[65] M. Kruk, M. Jaroniec, Gas adsorption characterization of ordered organic-inorganic nanocomposite materials, *Chemistry of Materials*, 2001, **13**, 3169-3183, doi: 10.1021/cm0101069.

[66] N. R. Palapa, T. Taher, B. R. Rahayu, R. Mohadi, A. Rachmat, A. Lesbani, CuAl LDH/Rice husk biochar composite for enhanced adsorptive removal of cationic dye from aqueous solution, *Bulletin of Chemical Reaction Engineering & Catalysis*, 2020, **15**, 525-537, doi: 10.9767/bcrec.15.2.7828.525-537.

[67] A. Y. Elnour, A. A. Alghyamah, H. M. Shaikh, A. M. Poulose, S. M. Al-Zahrani, A. Anis, M. I. Al-Wabel, Effect of pyrolysis temperature on biochar microstructural evolution, physicochemical characteristics, and its influence on biochar/polypropylene composites, *Applied Sciences*, 2019, **9**, 1149, doi: 10.3390/app9061149.

[68] R. Muzyka, E. Misztal, J. Hrabak, S. W. Banks, M. Sajdak, Various biomass pyrolysis conditions influence the porosity and pore size distribution of biochar, *Energy*, 2023, **263**, 126128, doi: 10.1016/j.energy.2022.126128.

[69] A. S. Singh, D. R. Naikwadi, K. Ravi, A. V. Biradar, Chemoselective isomerization of α-Pinene oxide to trans-Carveol by robust and mild Brønsted acidic zirconium phosphate catalyst, *Molecular Catalysis*, 2022, **521**, 112189, doi: 10.1016/j.mcat.2022.112189.

[70] Q. Fang, B. Chen, Y. Lin, Y. Guan, Aromatic and hydrophobic surfaces of wood-derived biochar enhance perchlorate adsorption *via* hydrogen bonding to oxygen-containing organic groups, *Environmental Science & Technology*, 2014, **48**, 279-288, doi: 10.1021/es403711y.

[71] W. K. Wakejo, B. T. Meshasha, J. W. Kang, Y. Chebude, Enhanced ciprofloxacin removal from aqueous solution using a chemically modified biochar derived from bamboo sawdust:

adsorption process optimization with response surface methodology, *Adsorption Science & Technology*, 2022, **2022**, 2699530, doi: 10.1155/2022/2699530.
[72] A. Downie, A. Crosky, P. Munroe, Physical properties of biochar. In Biochar for environmental management, Routledge, 2012, 45-64, ISBN: 9781849770552.
[73] F. Qin, C. Zhang, G. Zeng, D. Huang, X. Tan, A. Duan, Lignocellulosic biomass carbonization for biochar production and characterization of biochar reactivity, *Renewable and Sustainable Energy Reviews*, 2022, **157**, 112056, doi: 10.1016/j.rser.2021.112056.
[74] M. F. Gasim, Z. Y. Choong, P. L. Koo, S. C. Low, M. H. Abdurahman, Y. C. Ho, M. Mohamad, I. W. K. Suryawan, J. W. Lim, W. D. Oh, Application of biochar as functional material for remediation of organic pollutants in water: an overview, *Catalysts*, 2022, **12**, 210, doi: 10.3390/catal12020210.
[75] W. Yang, C. Lu, B. Liang, C. Yin, G. Lei, B. Wang, X. Zhou, J. Zhen, S. Quan, Y. Jing, Removal of Pb(II) from aqueous solution and adsorption kinetics of corn stalk biochar, *Separations*, 2023, **10**, 438, doi: 10.3390/separations10080438.
[76] R. Azargohar, A. K. Dalai, Biochar as a precursor of activated carbon, *Applied Biochemistry and Biotechnology*, 2006, **131**, 762-773, doi: 10.1385/ABAB:131:1:762.
[77] Y. Liu, J. Chen, Effect of ageing on biochar properties and pollutant management, *Chemosphere*, 2022, **292**, 133427, doi: 10.1016/j.chemosphere.2021.133427.
[78] R. Bardestani, G. S. Patience, S. Kaliaguine, Experimental methods in chemical engineering: specific surface area and pore size distribution measurements: BET, BJH, and DFT, *The Canadian Journal of Chemical Engineering*, 2019, **97**, 2781-2791, doi: 10.1002/cjce.23632.
[79] S. Ranganathan, Saravanan Rajendran, Lorena C. Ponce, Chemically modified carbon nanotubes for pollutants adsorption, chemically modified carbon nanotubes for commercial applications, 2023, 129-150, ISBN: 9783527350728.
[80] M. Gayathiri, T. Pulingam, K. T. Lee, K. Sudesh, Activated carbon from biomass waste precursors: Factors affecting production and adsorption mechanism, *Chemosphere*, 2022, **294**, 133764, doi: 10.1016/j.chemosphere.2022.133764.

Publisher's Note: Engineered Science Publisher remains neutral with regard to jurisdictional claims in published maps and institutional affiliations.

Open Access

This article is licensed under a Creative Commons Attribution 4.0 International License, which permits the use, sharing, adaptation, distribution and reproduction in any medium or format, as long as appropriate credit to the original author(s) and the source is given by providing a link to the Creative Commons license and changes need to be indicated if there are any. The images or other third-party material in this article are included in the article's Creative Commons license, unless indicated otherwise in a credit line to the material. If material is not included in the article's Creative Commons license and your intended use is not permitted by statutory regulation or exceeds the permitted use, you will need to obtain permission directly from the copyright holder. To view a copy of this license, visit http://creativecommons.org/ licenses/by/4.0/.

©The Author(s) 2025